J Mater Sci (2008) 43:557–567
DOI 10.1007/s10853-007-1779-3

5TH BRAZILIAN MRS MEETING

Purification of catalytically produced carbon nanotubes for use as support for fuel cell cathode Pt catalyst

Ana Maria Rocco · Cristiane A. da Silva · Maria I. F. Macedo · Luis Fernando Maestro · Marcelo H. Herbst · Guillermo Solórzano · Altair L. Xavier

Received: 30 January 2007 / Accepted: 13 April 2007 / Published online: 29 June 2007

Abstract A purification method based on HCl treatment under reflux was employed for purification of carbon nanotube (CNT) samples, obtained by the electric discharge method utilizing $Zr(Co_{0.5}Ni_{0.5})_2$, $Ce_3(Co_{0.5}Ni_{0.5})_2$ and $Ce(Co_{0.5}Ni_{0.5})_5$ as catalysts. Raman Spectroscopy provided information on the SWCNT presence in the untreated samples. Scanning Electron Microscopy (SEM) showed CNT with different diameters and lengths. Different acid treatment conditions were employed and the best results were achieved for HCl 3 mol/L aqueous solution during 24 h reflux. Transmission Electron Microscopy (TEM) images, associated with EDS, revealed the catalyst removal from the original sample and the presence of other carbon structures near the CNT formation. CNT acid functionalization for Pt nanoparticles dispersion was successful, resulting in a homogeneously dispersed system, as seen in TEM images. Temperature Programmed Oxidation (TPO) analysis of the raw and purified samples indicated that after purification there are three different carbon species present on the purified material, each one showing a different behavior towards O_2 oxidation.

A. M. Rocco (✉) · C. A. da Silva · M. I. F. Macedo · A. L. Xavier
Grupo de Materiais Condutores e Energia, Escola de Química, Universidade Federal do Rio de Janeiro, Centro de Tecnologia, Cidade Universitária, RJ 21941-909, Brasil
e-mail: amrocco@eq.ufrj.br

L. F. Maestro
Instituto de Física Gleb Wataghin – IFGW, UNICAMP, Campinas, SP, Brasil

M. H. Herbst
Universidade Federal Rural do Rio de Janeiro, UFRRJ, Seropédica, RJ, Brasil

G. Solórzano
Department of Materials Science and Metallurgy, Pontifícia Universidade Católica – PUC-Rio, Gávea, Rio de Janeiro, RJ 23453-900, Brasil

Introduction

The unique structural, electronic and mechanical, among other properties of carbon nanotubes [1, 2,] stimulate their use in a wide spectrum of advanced applications in nanotechnology such as electronic and electro-mechanical nanodevices [2–4]. In addition, the very high aspect ratio and high conductivity of carbon nanotubes make them ideal building blocks for high strength and directional conductive composites [5]. Single-walled carbon nanotubes (SWNTs) are expected to have a wide range of practical applications such as catalyst supports in heterogeneous catalysis, field emitters, sensors, gas-storage media and molecular wires for next generation electronic devices [6–8].

While the scientific and technological potential of SWNTs has attracted considerable attention in the recent years, progress in this field is currently inhibited by the difficulty of synthesizing sufficient amounts of high-quality and high-purity materials. There are several methods for obtaining SWNTs, from electric arc discharge and laser ablation of metal-containing carbon targets to direct decomposition of carbon-containing molecules over metal catalysts [9–12]. Among the different alternatives for SWNTs production, the catalytic decomposition of carbon-containing molecules is one of the most promising technique, due to the low cost scale-up possibility, which enables applications that require large SWNT amounts [13]. However,

the raw material obtained by any of the mentioned methods contains different concentrations of carbon impurities such amorphous carbon, graphite fibers as well as residual metals from the catalyst used in the production [14–17]. Hence, a crucial step on the production of SWNTs is a systematic characterization of the type and concentration of contaminants present on a given nanotube sample. Filtration, centrifugation and chromatographic techniques are purification methods usually employed for impurity elimination, which consists, in general, of trace amounts of catalyst, nanoparticles, and amorphous carbon, after the SWNTs have been treated with acid or oxidizing agents [18–20].

Analytical Electron Microscopy (AEM) techniques, Thermo Gravimetric analysis (TGA), Raman Spectroscopy and Temperature Programmed Oxidation (TPO) have been used to obtain mostly qualitative assessments of the various carbon species present on a given SWNT sample and a quantitative measurement of the overall concentration of residual metals, respectively [21–23]. Herrera and co-workers proposed the TPO method as a useful tool for quantifying the amount of SWNT present on a sample [20], due to the narrow temperature range in which the catalyst-embedded SWNT burn, and, below the temperature in which MWNT, graphite, and carbon fibers are oxidized, but above the temperature at which amorphous carbon species are oxidized [5].

Our interest in SWNTs is their application as catalyst supports for Pt in a proton exchange membrane fuel cell (PEMFC). We have applied different purification methods to different carbon nanotube-containing systems, searching for a purification procedure of SWNTs to be used as catalyst Pt support.

The aim of the present work is to study a method for purification and characterization of a CNT (carbon nanotube) sample, for application as catalyst support in a fuel cell. Temperature Programmed Oxidation (TPO) and Raman Spectroscopy were used as quantitative and qualitative techniques for determination of raw and purified CNT samples obtained by the electric discharge method under He atmosphere, employing $Ce_3(Co_{0.5}Ni_{0.5})_2$, $Ce(Co_{0.5}Ni_{0.5})_5$ and $Zr(Co_{0.5}Ni_{0.5})_2$ catalysts. Samples were also analyzed by Scanning Electron Microscopy (SEM), and Transmission Electron Microscopy (TEM) in order to characterize their morphology, structure, size distribution and local composition.

Experimental section

Syntheses

The CNT samples used in the present work were previously prepared from high purity graphite (Carbon of America UF-4S) utilizing the electric discharge method under He atmosphere, employing $Zr(Co_{0.5}Ni_{0.5})_2$, $Ce_3(Co_{0.5}Ni_{0.5})_2$ e $Ce(Co_{0.5}Ni_{0.5})_5$ as catalysts. The CNT were produced in the plasma formed during the pyrolysis of the graphite anode doped with the catalyst, and deposited at the graphite cathode. A current of 120 A (d.c.) and a He pressure of 400 Torr were applied during the syntheses.

Sample treatment

The CNT were prepared by the arc discharge method as described previously and characterized by Raman spectroscopy, Scanning Electron Microscopy (SEM) and Transmission Electron Microscopy (TEM), both of two with simultaneous X-ray Dispersive Energy (EDS), and Temperature Programmed Oxidation (TPO). The different raw samples (30 mg) were suspended in 50 mL of HCl solutions of 0.5, 3.0 mol/L and concentrated (reagent grade), treated under ultra-sound during 30 min and the mixtures heated at reflux (80 °C) during 24 h and 36 h. After slow cooling to room temperature, the supernatant was removed and the solid was re-suspended in deionized water, filtered through a 0.45 μm filter membrane (polycarbonate, Millipore) and washed with deionized water and a 10% NH_4OH aqueous solution up to attaining a constant pH (7). The solid was dried under vacuum at constant weight resulting in about 15 mg of sample. After dried the samples were characterized by SEM, TEM and EDS.

The sample originally obtained using $Ce_3(Co_{0.5}Ni_{0.5})$ and treated using 3.0 mol/L HCl solution was additionally treated by TPO, for analysis of the carbon forms present in the sample after purification. This sample was either funcionalizated using the mixture of H_2SO_4/HNO_3 solution for dispersion of Pt nanoparticles.

H_2SO_4/HNO_3 functionalization and Pt deposition

After the acid purification with HCl 3 mol/L solution, the CNT functionalization was carried out in order to allow the Pt dispersion at the CNT surface, adding 30 mg of the sample to a flask containing 5 mL of a 4 mol/L H_2SO_4/HNO_3 solution under stirring and heating during 4 h. The suspension formed was filtered in a 0.45 μm porous membrane and the solid dried under vacuum.

In order to obtain a Pt dispersion at the CNT surface, 70 mL of a H_2PtCl_6 solution in ethylene glycol (20% weight in Pt) was added to the CNT sample and the system was kept under reflux during 6 h, filtered and the solid dried under vacuum. A Vulcan XC-72R carbon sample was submitted to a similar procedure for comparison and control. A 1 g carbon sample was added to 10 mL of a 4 mol/L H_2SO_4/HNO_3 solution under stirring and heating during

4 h, and the further steps were identical to those employed for the CNT sample.

Samples characterization

Raman spectra were obtained using a Jobin–Yvon T64000 triple monochromator (in the double subtractive configuration) equipped with an Olympus microscope and a liquid-N_2 cooled detector. The 514.5 nm (2.41 eV) line of an argon ion laser was employed as excitation. The laser power was kept below 20 mW to prevent heating the samples. All measurements were carried out at room temperature in the backscattering geometry. The silicon Raman line was used for calibration purposes.

SEM analyses were performed in a Zeiss DSM 940 microscope. CNT samples were dispersed in propanol and treated under ultrasound during 12 min. Drops of this dispersion were cast on an Al sample holder, followed by vacuum drying and metallization.

TEM analyses were performed in a JEOL 2010 microscope, operating at 200 kV under diffraction contrast and phase contrast modes. Bright and dark field images were documented, together with their correspondent selected area diffraction patterns, allowing high contrast micrographs at nanometric scale. Under given sample orientations respect the incident electron beam, phase contrast allowed the observation of CNT and metal particles lattice planes. CNT samples were dispersed in isopropanol and treated under ultrasound during 10 min and drops of the dispersions were cast on copper gauze and dried under vacuum.

TPO analyses were performed in a flux equipment with 22.23 μL looping and a U-shape quartz microreactor in a multi-purpose unit coupled to a Balzers QMS-422 quadrupole mass spectrometer. CNT samples were heated from 25 °C up to 800 °C at 10 °C/min under O_2/He (5% in O_2) 10 mL/min flux. Calibration of the equipment was performed measuring known volumes of N_2 and CO_2.

Results and discussion

Raman spectroscopy

Raman spectroscopy has proved to be a powerful technique for nanotube characterization. The Raman-allowed phonon mode E_{2g}, has extensively been used as a measure of the presence of ordered carbon, while the so-called D band is related to defects or the presence of nanoparticles and amorphous carbon [24, 25]. The intensity of the D-band relatively to the G-band can be used as a qualitative measurement of the presence of carbon forms other than nanotubes. However, for an accurate quantitative determination of the different carbon species present in a given sample, techniques other than Raman must be employed.

Figures 1 and 2 exhibit, illustratively, the Raman spectra collected for CNT samples synthesized with $Ce(Co_{0.5}Ni_{0.5})_5$ catalyst in the spectral region between 100 cm^{-1} and 400 cm^{-1} and between 1200 cm^{-1} and 1800 cm^{-1}. The vibrational modes observed in the region between 100 cm^{-1} and 300 cm^{-1}, called radial breathing modes (RBM) [26] exhibit A_{1g} symmetry and are inversely proportional to the nanotube diameter, not depending on its quirality. This band is formed by overlapping of individual peaks associated with single nanotubes whose relative intensity strongly depends on the energy of the incident laser beam.

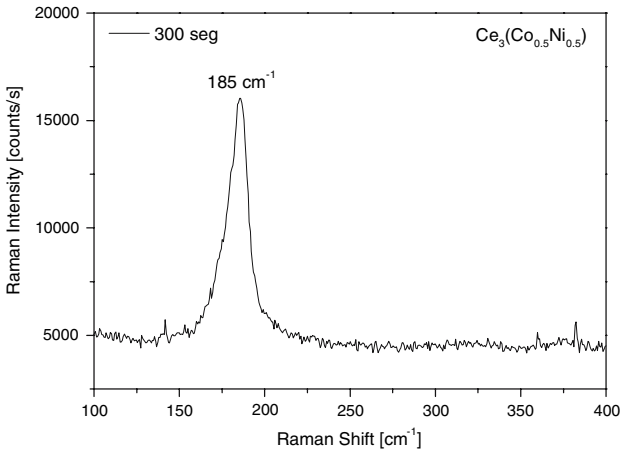

Fig. 1 Raman spectrum of CNT samples synthesized with $Ce_3(Co_{0.5}Ni_{0.5})$ catalyst in the region between 100 cm^{-1} and 400 cm^{-1}

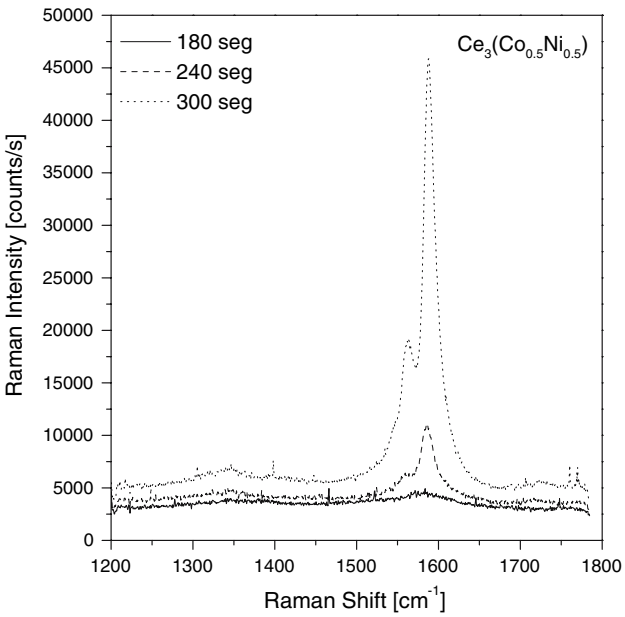

Fig. 2 Raman spectra of CNT samples synthesized with $Ce_3(Co_{0.5}Ni_{0.5})$ catalyst in the region between 1200 cm^{-1} and 1800 cm^{-1}

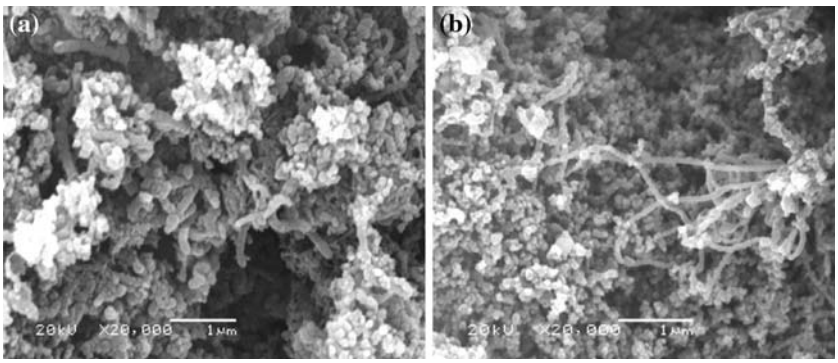

Fig. 3 (**a**) and (**b**) SEM images of the untreated CNT sample synthesized with the $Zr(Co_{0.5}Ni_{0.5})_2$ catalyst in different regions

Tangential vibrational modes are responsible for the G-band, near 1575 cm^{-1}, which is associated with defect-free nanotubes. This band presents a weak dependence on the CNT diameter and does not depend on the laser excitation energy between 0.94–1.59 eV and 2.41–3.05 eV. The D-band, attributed to disordered structures, such as defective CNT and amorphous carbon, is usually found at 1350 cm^{-1} [1].

Figure 2 shows the Raman spectra obtained at different acquisition times, in the region between 1200 cm^{-1} and 1800 cm^{-1}. The most important bands are observed even in short acquisition times, however, the shoulder at 1575 cm^{-1}, which evidences the presence of metallic CNT is observed only at 180 s. A peak centered at 1600 cm^{-1}, attributed to the tangential mode (G-band), associated with perfect CNT, as well as the D-band, at 1350 cm^{-1}, associated with disordered structures, such as amorphous carbon and defective CNT are also observed.

In Fig. 2, at 180 s acquisition time, a band centered at 185 cm^{-1} is clearly seen, characteristic of the radial breathing vibrational mode. Only single-walled carbon nanotubes (SWCNT) exhibit radial breathing mode, which confirms the presence of such CNT in the synthesized sample. Multi-walled CNT (MWCNT) does not exhibit radial breathing bands in Raman spectra, however, Benoit and co-workers [27] found low-frequency bands in MWCNT samples. This feature can be observed only in high-quality, high-purity MWCNT samples, in which the internal diameter is smaller than 2 nm. The Raman analysis in the present work was interpreted merely as a qualitative tool, aiming the identification of the CNT and to prove the existence of SWCNT. All the spectra collected exhibited bands that identify the SWCNT in the samples, as well as other less-ordered carbon structures.

Morphological characterization

The direct characterization of CNT can be appropriately performed employing Scanning and Transmission Electron Microscopy (SEM and TEM, respectively). SEM images provide morphological and homogeneity information of the synthesized CNT, and also a qualitative measure of the efficiency of the synthesis, purification and functionalization steps. TEM images allow detailed structural studies of CNT samples, from which the presence of metal nanoparticles (encapsulated or at the CNT surface) can be detected. While TEM images possess higher resolution, SEM has the advantage of allowing topological analyses and construction of three-dimensional images.

X-ray Dispersive Energy (EDS) is an important technique for the microscopic characterization of materials, which allow element identification in specific sample regions. The technique also allows mapping of element distribution, which provides compositional maps of selected elements.

Figures 3 and 4 show representative SEM images and a EDS spectra of the CNT sample synthesized with $Zr(Co_{0.5}Ni_{0.5})_2$ catalyst, before the chemical treatment. The CNT sample shown in Fig. 3(a) and (b) exhibit nanotube formations [28] of different lengths and diameters, with high heterogeneity, amorphous carbon formations (rounded

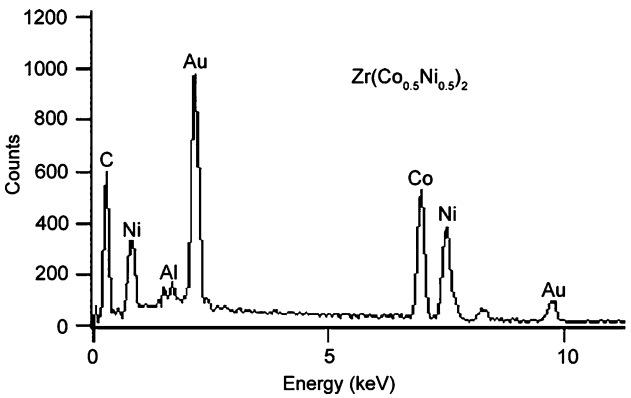

Fig. 4 EDS spectrum of the untreated CNT sample synthesized with the $Zr_2(Co_{0.5}Ni_{0.5})$ catalyst

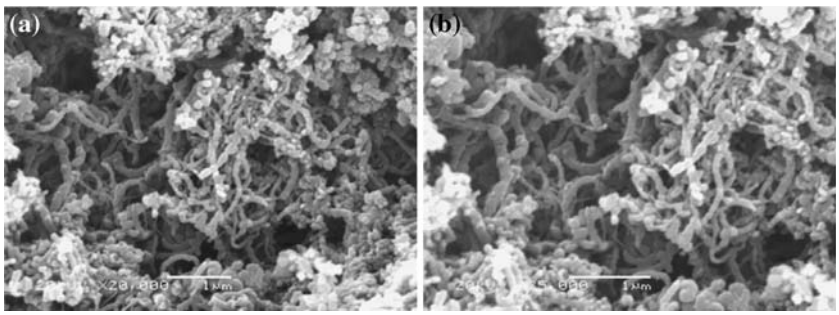

Fig. 5 (**a**) and (**b**) SEM images (in different regions) of the CNT sample synthesized with the $Zr(Co_{0.5}Ni_{0.5})_2$ catalyst and treated with concentrated HCl during 24 h

grey form) and catalyst particles (white) smaller than 1 μm. The CNT diameter in Fig. 3(a) and (b) is approximately 166 nm and 80 nm, respectively. CNT fibers originated from a catalyst aggregate observed in Fig. 3(b) are morphological formations expected for samples obtained with the majority of the synthesis methods, which generate large amounts of carbon with different morphologies. Exceptions are the methods which promote CNT growing from nanoporous materials.

From the EDS spectra, in Fig. 4, the metals Co and Ni from the catalyst can be clearly identified. Al and Au peaks are originated from the support and the metallization process, respectively.

Figures 5–8 show SEM images and EDS spectra of the CNT sample obtained with the $Zr(Co_{0.5}Ni_{0.5})_2$ catalyst, treated with concentrated HCl during 24 h and 36 h.

In Fig. 5, metallic catalyst aggregates are observed, however, smaller than those found for the untreated sample. The decrease in the size of amorphous carbon formations is also observed. The EDS spectrum of Fig. 6 exhibits Co and Ni peaks with lower intensity, comparatively to the untreated sample. However, a considerable catalyst amount can be seen in the image.

CNT sample treatment during 36 h damaged the nanotubes, which were shortened, as seen in Fig. 7. The EDS spectra (Fig. 8) did not exhibit Co and Ni peaks, which are probably present in concentrations lower than 1%. Similar results were found for the other catalysts utilized. Despite the fact that HCl purification is currently employed for catalyst removal and little effect on the carbon formations is reported [29], exposition of the

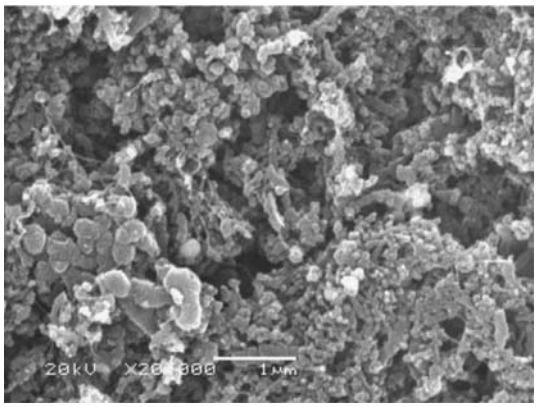

Fig. 7 SEM image of the CNT sample synthesized with the $Zr(Co_{0.5}Ni_{0.5})_2$ catalyst and treated with concentrated HCl during 36 h

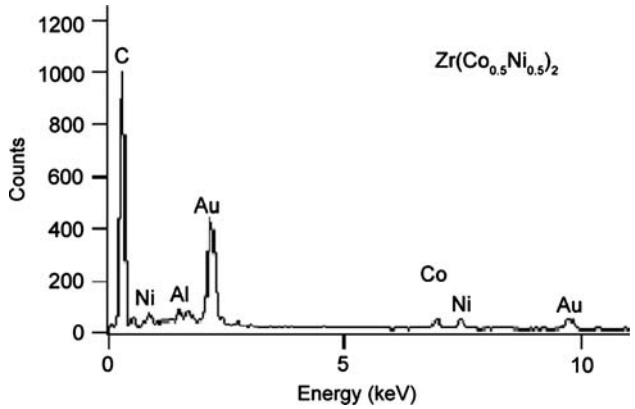

Fig. 6 EDS spectrum of the CNT sample synthesized with the $Zr(Co_{0.5}Ni_{0.5})_2$ catalyst and treated with concentrated HCl during 24 h

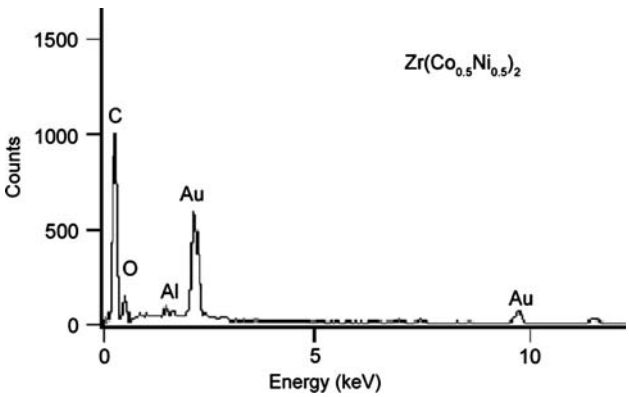

Fig. 8 EDS spectrum of the CNT sample synthesized with $Zr(Co_{0.5}Ni_{0.5})_2$ catalyst and treated with concentrated HCl during 36 h

sample to longer times in HCl concentrated solution damaged the CNT.

Samples obtained with the three catalysts employed were also treated with HCl 0.5 mol/L solution and this concentration was not effective for metal removal, while 3 mol/L [30, 31] presents results similar to the utilization of concentrated HNO_3 [32]. HCl 3 mol/L solution was utilized, since more concentrated solutions cause damage to the CNT. TEM images of the CNT obtained with cerium catalysts treated under these conditions are illustratively shown and this sample was chosen for the Pt dispersion characterizations.

TEM study of the CNT sample synthesized with $Ce_3(Co_{0.5}Ni_{0.5})$ catalyst

CNT samples obtained with $Ce_3(Co_{0.5}Ni_{0.5})$ catalyst were purified employing the method described, with 3 mol/L HCl during 24 h reflux. Figure 9 shows the TEM images for the CNT original sample (untreated) obtained with the $Ce_3(Co_{0.5}Ni_{0.5})$ catalyst. Figure 9(a) shows the bright field image of the Ni-rich particle, (b) and (c) are dark field images with two different reflections, (d) is the corresponding selected area electron diffraction pattern and (e) the EDS of the CNT sample.

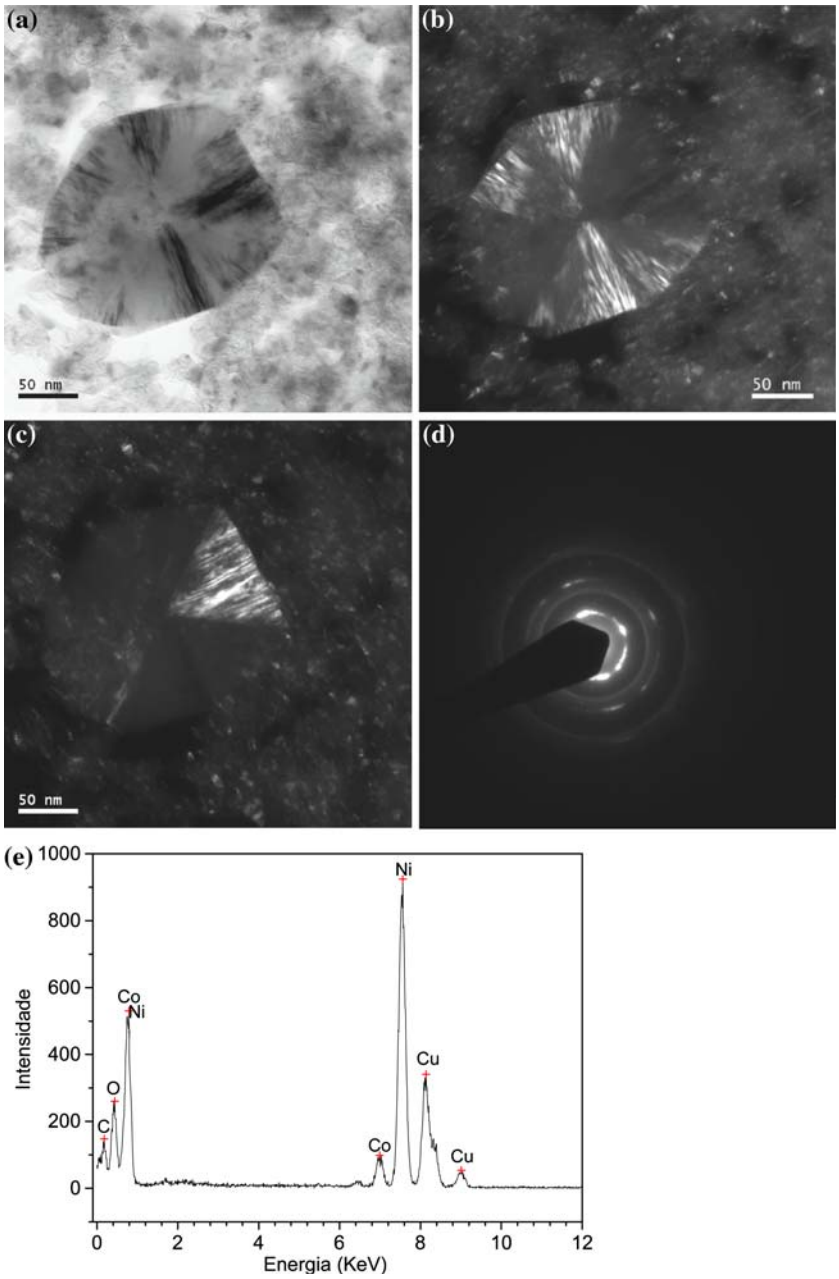

Fig. 9 TEM images of the CNT sample obtained with the $Ce_3(Co_{0.5}Ni_{0.5})$ catalyst: (**a**) bright field image showing the Ni-rich particle, (**b**) and (**c**) are dark field images centered in different beams, (**d**) electron diffraction image and (**e**) EDS spectrum of the nanoparticle, exhibiting Ni and Co peaks

As observed in the figure, a large metallic particle of approximately 150 nm diameter is prominent in comparison with smaller, on the order of 10 nm, dispersed particles, Fig. 9(a–c). EDS analysis have shown that the larger is a nickel-rich particle and the smaller ones are mainly cobalt originated from the catalyst. The Cu peak observed in the EDS spectra is associated with the copper supporting grid. The electron diffraction image in Fig. 9(d) displays concentric rings, indicating the polycrystalline behavior of the sample.

Figure 10 shows TEM images of the CNT sample synthesized with the $Ce_3(Co_{0.5}Ni_{0.5})$ catalyst and purified with 3 mol/L HCl solution. Catalyst-free CNT samples can be observed in Fig. 10(a) and a graphite layered formation parallel to the CNT, with layer distance of 0.43 nm is also observed. Deng and co-workers [33] observed similar formations in CNT samples with Cu obtained by hydrothermal synthesis, in which the layer distance was 0.33 nm. The graphite layers region, in detail, is shown in Fig. 10 (b). The EDS spectrum of the CNT sample is shown in Fig. 10(d), in which a peak associated with carbon species is observed, as well as Cu peaks, associated with the copper support. Two low intensity peaks near the C peak can be associated with residual Ni and Co, however, it is most probably noise, due to the very low intensity of the signal.

Comparison of peak intensity in the EDS spectra of untreated and treated samples evidences compositional variations of the catalysts, confirming the metal removal from the CNT sample after purification. This indicates the efficacy of the method for metal catalyst removal.

CNT functionalization with H_2SO_4/HNO_3 was carried out aiming the introduction of acid groups, since they act as high homogeneity nucleation centers for Pt coordination in the CNT surface. TEM images showed that the functionalization method probably damaged part of the CNT in the sample, since a considerable amount of Pt nanoparticles was found deposited on non-CNT carbon formations. Figure 11(a) shows a bright field image of the Pt nanoparticles, with about 5 nm diameter, deposited on carbon (probably amorphous) regions. A dark field image of the other region is shown in Fig. 11(b) and (c) exhibits the electron diffraction pattern, indicating the polycrystalline nature of the sample. Concentric rings are indexed and correspond to Pt particles diffracting planes (111), (200), (220) and (311) [34]. Corroborating these observations, intense Pt peaks are observed in the EDS spectrum, shown in Fig. 11(d) and the Cu peak is associated with copper support.

Temperature Programmed Oxidation (TPO)

The previous results indicated that, after the CNT functionalization, the total amount of CNT in the sample decreases, as shown by TEM images. In this regard, TPO

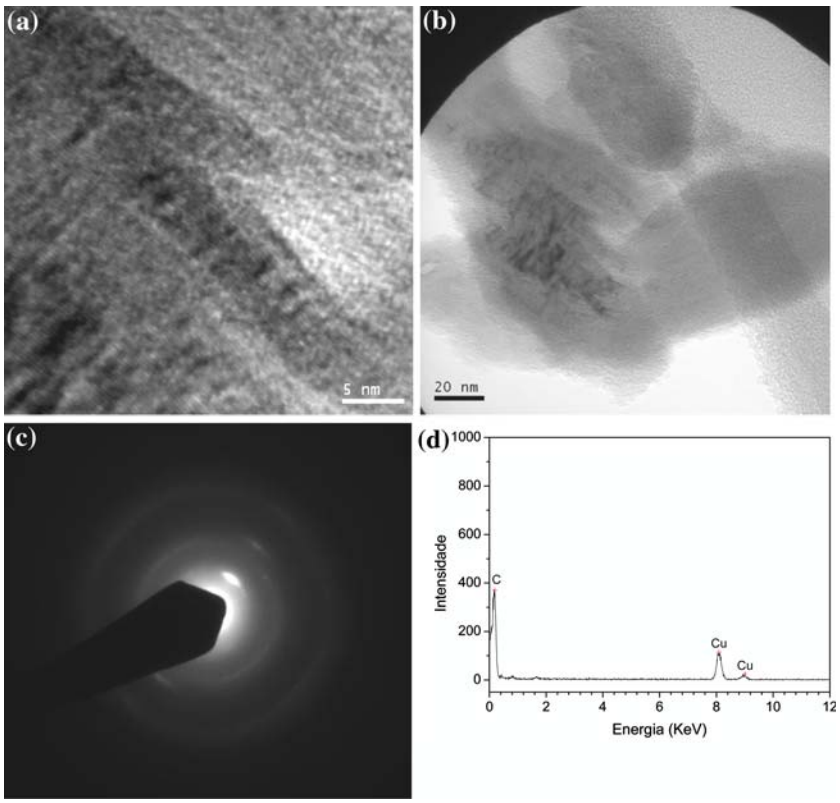

Fig. 10 TEM image of the CNT sample obtained with the $Ce_3(Co_{0.5}Ni_{0.5})$ catalyst after purification: (**a**) Catalyst-free CNT and ordered graphite layer region, (**b**) graphite layer region in detail, (**c**) electron diffraction image and (**e**) EDS spectrum of the graphite region, where Ni and Co peaks are absent

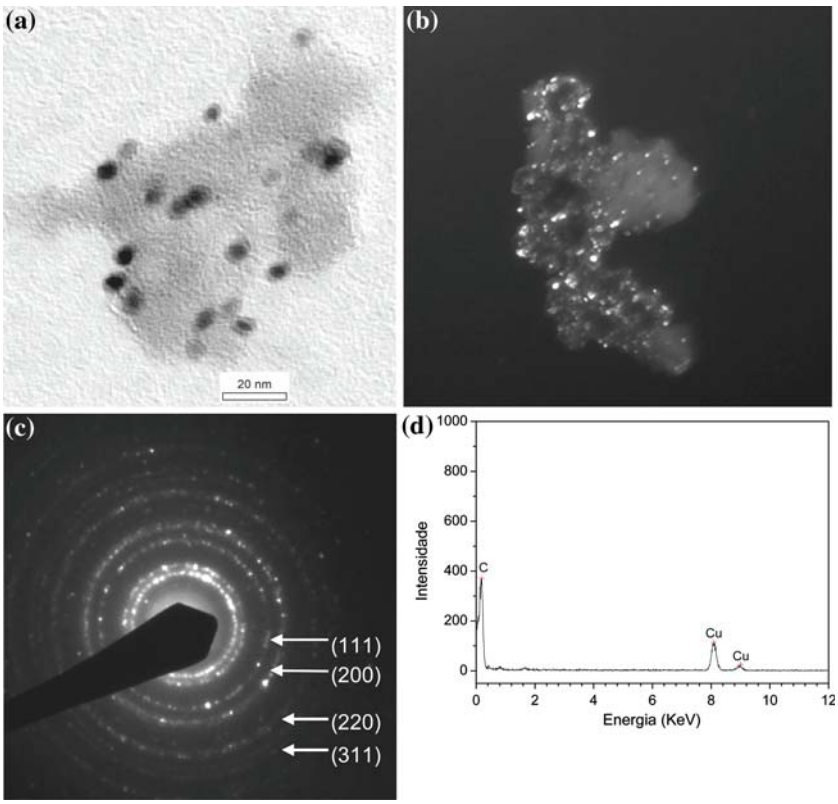

Fig. 11 TEM images of the 20%Pt/CNT sample (**a**) bright field (**b**) dark field in different regions (**c**) electron diffraction image and (**d**) EDS spectrum of the sample

technique was employed to characterize the system. TPO appears particularly suitable for the quantitative characterization of SWNT because SWNT are oxidized in a relatively narrow temperature range, which lies above the temperature of oxidation of amorphous carbon and below the oxidation of MWNT and graphitic carbon [35].

In the present study, CNT/$Ce_3(Ni_{0.5}Co_{0.5})$, CNT/$Ce(Ni_{0.5}Co_{0.5})_5$ and purified CNT/$Ce_3(Ni_{0.5}Co_{0.5})$ samples were characterized by TPO. The system was heated up to 800 °C with a 10 °C/min rate under 10 mL/min O_2/He (5% in O_2) flux. At this temperature, a 20 min isotherm was performed.

Figure 12 presents TPO profiles for CNT/$Ce_3(Ni_{0.5}Co_{0.5})$, CNT/$Ce(Ni_{0.5}Co_{0.5})_5$ and purified CNT/$Ce_3(Ni_{0.5}Co_{0.5})$ samples.

Shape and position of TPO peaks vary with catalyst composition and the oxidation kinetics. According to Kitiyanan and co-workers [35], amorphous and chemically impure carbon species are oxidized at temperatures below 400 °C, consequently subsequent oxidation steps remove increasing amounts of amorphous carbon material from the samples.

TPO profile of the CNT/$Ce(Ni_{0.5}Co_{0.5})_5$ sample presented two distinct peaks, at 447 °C and 655 °C, while for

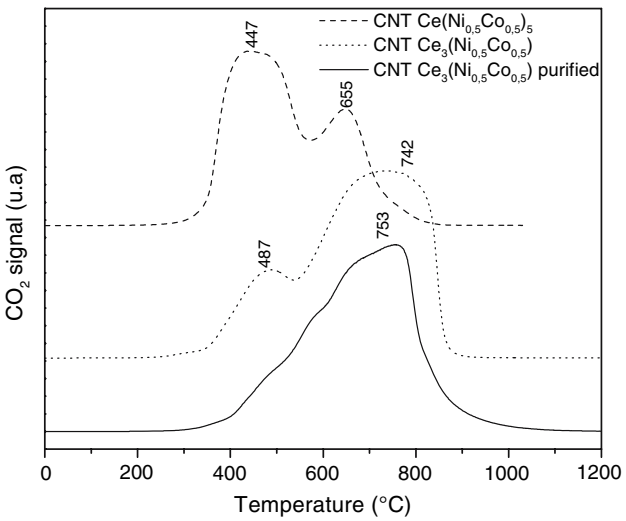

Fig. 12 TPO curves of the carbon species present in the CNT samples

CNT/$Ce(Ni_{0.5}Co_{0.5})_5$ sample, the TPO profile exhibited peaks centered at 487 °C and 742 °C.

TPO profiles of untreated samples presented significant differences in peak intensities, with inversion of relative

intensity for samples CNT/$Ce_3(Ni_{0.5}Co_{0.5})$ and CNT/$Ce(Ni_{0.5}Co_{0.5})_5$. The amount of metal catalyst utilized in the CNT synthesis is known to influence markedly on the different carbon species production and, consequently, on the peak shift in TPO profiles [9, 36]. Apparently, the higher Ni and Co concentration (CNT/$Ce(Ni_{0.5}Co_{0.5})_5$ sample) provides a higher amorphous carbon fraction, since the 447 °C possesses higher intensity and area. However, TPO is a catalytic process in which residual metals can have a significant impact. On the untreated material, the amount of Ni and Co is so high that all the different forms of carbon in the sample can be easily oxidized simultaneously at lower temperatures. Herrera and co-workers [9] used TPO coupled with Raman spectroscopy for the identification of the species evolved from the oxidation process at each peak present in the TPO profile. They found that, despite the oxidation treatments, amorphous carbon was preferentially eliminated, being clear that different peaks observed in the sample do not correspond to different carbon species, being also possible peaks associated with CNT/catalysts.

In order to separate the different contributions of carbon structures in samples studied in the present work, decomposition of TPO curves in Gaussian functions was performed. Figures 13–15 show the decomposition results, evidencing the different carbon forms contributing to the TPO profile. In these curves, CO_2 flux is monitored as a function of the temperature.

The acid treatment utilized in the CNT sample synthesized with the $Ce_3(Ni_{0.5}Co_{0.5})$ catalyst eliminated great part of the amorphous carbon, as observed in the TPO curve, with a lower temperature peak.

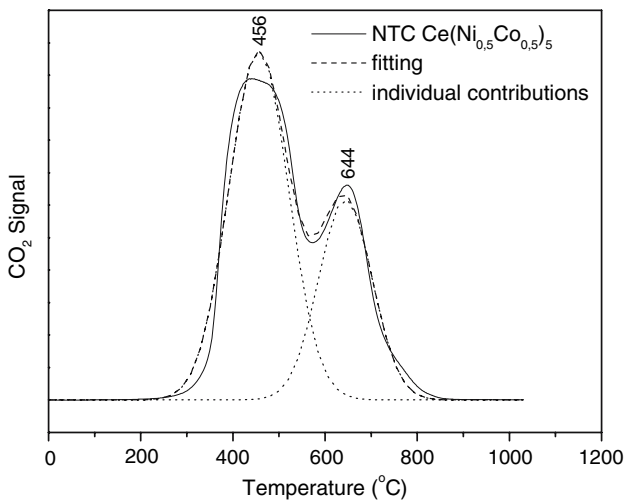

Fig. 13 Decomposition of TPO curves in Gaussian functions: untreated CNT sample synthesized with $Ce(Ni_{0.5}Co_{0.5})_5$ catalyst

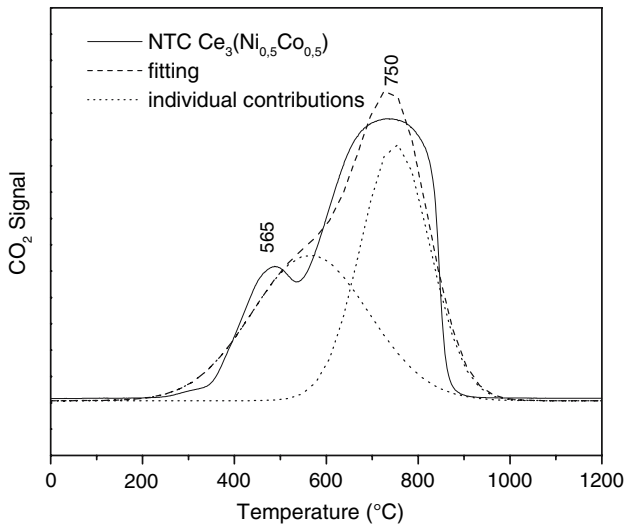

Fig. 14 Decomposition of TPO curves in Gaussian functions: untreated CNT sample synthesized with $Ce_3(Ni_{0.5}Co_{0.5})$ catalyst

From the signal decomposition of TPO curves into Gaussian functions, also based on the Raman, TEM and EDS results, two contributions were found for untreated samples and three for the purified one. The different fractions and attributions are listed in Table 1.

From the Table 1, a comparison between untreated and purified sample profiles indicated that after purification there are three different carbon species present on the purified material, each one showing a different behavior towards O_2 oxidation. Catalysts were not detected in the purified sample by EDS or TEM than, if there is any presence of metals in the sample, their concentration is less

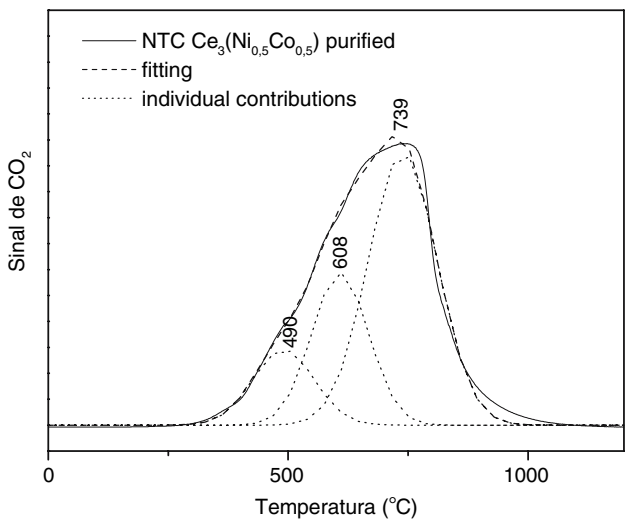

Fig. 15 Decomposition of TPO curves in Gaussian functions: CNT sample synthesized with $Ce_3(Ni_{0.5}Co_{0.5})$ catalyst and treated with 3 mol/L HCl solution

Table 1 Carbon fractions in CNT samples

Sample	Carbon fractions from TPO curves			
	Amorphous carbon + CNT/catalyst	CNT	Graphite	CNT + graphite
CNT/$Ce(Ni_{0.5}Co_{0.5})_5$	65.9	–	–	34.1
CNT/$Ce_3(Ni_{0.5}Co_{0.5})$	45.5	–	–	54.5
Purified CNT/$Ce_3(Ni_{0.5}Co_{0.5})$	14.5	27.0	58.5	–

than 1%. Results indicate that the peak at 490 °C (14.5%) corresponds to amorphous carbon or CNT/catalyst (residual), the peak at 608 °C (27.0%) is associated to CNT and at 739 °C (58.5%) graphite. The oxidation of this carbon form occurred at very high temperatures, with onset at about 700 °C, and completed after 30 min at 800 °C. The TPO attributions are based either on the analyses of standard graphite samples which exhibited oxidation peaks at temperatures higher than 650 °C and commercial SWNT samples from Tubes@Rice showed peaks centered at 550 °C [35]. The presence of graphite structures was shown previously in the TEM analyses.

Conclusion

In summary, purification treatment of CNT with HCl shown that concentrated acid solutions remove the metallic catalyst but damage the CNT, especially at long time under reflux. Utilization of moderated acid concentrations (about 3 mol/L) results in the removal of almost all catalyst and some extent of amorphous carbon with 24 h reflux. All the samples analyzed contained SWCNT, according to Raman results, and the Ce-based catalysts showed great amorphous carbon contributions with the increase in the concentration of Co and Ni. Analytical microscopy provided information of the morphology and purity of CNT samples and supported the results of TPO analyses, which indicated a greater fraction of graphite in the sample and a low fraction of CNT. CNT acid functionalization for Pt nanoparticles dispersion was successful, resulting in a homogeneously dispersed system, as seen in TEM images.

Acknowledgments Authors would like to thank CNPq for fellowships and financial support of the present work (CNPq/CT/Energ Nos 50.4222/2004-0 and 40.1494/2003-9) and FAPERJ (E-26/170.700/2004), "Grupo de Combustíveis Alternativos" at IFGW (UNICAMP) for the CNT samples and NUCAT/UFRJ for TPO analyses. CAS thanks Agência Nacional do Petróleo (ANP) for scholarship.

References

1. Tzitzios V, Georgakilas V, Oikonomou E, Karakassidesb M, Petridis D (2006) Carbon 44:848
2. Baughman RH, Zakhidov AA, De Heer WA (2002) Science 297:787
3. Kong J, Franklin NR, Zhou C, Chapline MG, Peng S, Cho K et al (2000) Science 287:622
4. Postma HWC, Teepen T, Yao Z, Grifoni M, Dekker C (2001) Science 293:76
5. Ajayan PM, Schadler LS, Giannaris C, Rubio A (2000) Adv Mater 12:750
6. Waje MM, Wang X, Li W, Yan Y (2005) Nanotechnology 16:S395
7. Ye JS, Wen Y, Zhang WD, Gan LM, Xu GQ, Sheu FS (2004) Electrochem Commun 6:66
8. He PG, Dai LM (2004) Chem Commun 3:348
9. Herrera JE, Resasco DE (2003) Chem Phys Lett 376:302
10. Nikolaev P, Bronikowski MJ, Bradley RK, Rohmund F, Colbert DT, Smith KA, Smalley RE (1999) Chem Phys Lett 313:91
11. Kong JA, Cassell AM, Dai H (1998) Chem Phys Lett 292:567
12. Rana RK, Koltypin Y, Gedanken A (2001) Chem Phys Lett 344:256
13. Resasco DE, Alvarez WE, Pompeo F, Balzano L, Herrera JE, Kitiyanan B, Borgna A (2002) J Nanoparticle Res 4:131
14. Peigney A, Coquay P, Flahaut E, Vandenberghe RE, De Grave E, Laurent C (2001) J Phys Chem B 105:9699
15. Zhao B, Hu H, Niyogi S, Itkis ME, Hamon MA, Bhowmik P, Meier MS, Haddon RC (2001) J Am Chem Soc 123:11673
16. Yang CM, Kaneko K, Yudasaka M, Iijima S (2002) Nano Lett 2:385
17. Lobach AS, Spitsina NG, Terekhov SV, Obraztsova ED (2002) Phys Solid State 44:475
18. Niyogi S, Hu H, Hamon MA, Bhowmik P, Zhao B, Rozenzhak SM, Chen J, Itkis ME, Meier MS, Haddon RC (2001) J Am Chem Soc 123:733
19. Liu J, Rinzler AG, Dai H, Hafner JH, Bradley RK, Boul PJ, Lu A, Iverson T, Shelimov K, Huffman CB, Rodriguez-Macias F, Shon Y-S, Lee TR, Colbert DT, Smalley RE (1998) Science 280:1253
20. Holzinger M, Hirsch A, Bernier P, Duesberg GS, Burghard M (2000) Appl Phys A 70:599
21. Rao CNR, Satishkumar BC, Govindaraj A, Nath M (2001) Chem Phys Chem 2:78
22. Rinzler AG, Liu J, Dai H, Nikolaev P, Huffman CB, Rodriguez-Macias FJ, Boul PJ, Lu AH, Heymann D, Colbert DT, Lee RS, Fischer JE, Rao AM, Eklund PC, Smalley RE (1998) Appl Phys A 67:29
23. Shi Z, Lian Y, Liao F, Zhou X, Gu Z, Zhang Y, Ijima S (1999) Solid State Commun 112:35
24. Saito R, Fujita M, Dresselhaus G, Dresselhaus MS (1992) Appl Phys Lett 60:2204
25. Alvarez WE, Pompeo F, Herrera JE, Balzano L, Resasco DE (2002) Chem Mater 14:1853
26. Herbst MH, Macêdo MIF, Rocco AM (2004) Química Nova 27:986
27. Benoit JM, Buisson JP, Chauvet O, Godon C, Lefrant S (2002) Phys Rev B 66:073417
28. Moon JM, An KH, Lee YH, Park YS, Bae DJ, Park GS (2001) J Phys Chem B 105:5677
29. Chiang IW, Brinson BE, Smalley RE, Margrave JL, Hauge RH (2001) J Phys Chem B 105:1157

30. Harutyunyan AR, Pradhan BK, Chang J, Chen G, Eklund PC (2002) J Phys Chem B 106:8671
31. Endo M, Lee BJ, Kim YA, Kim YJ, Muramatsu H, Yanagisawa T, Hayashi T, Terrones M, Dresselhaus MS (2003) New J Phys 5:121
32. Bandow S, Rao AM, Williams KA, Thess A, Smalley RE, Eklund PC (1997) J Phys Chem B 101:8839
33. Deng B, Xu A-W, Chen GY, Song R-Q, Chen L (2006) J Phys Chem B 110:11711
34. Zhang L, Samulski ET (2004) Chem Phys Lett 398:505
35. Kitiyanan B, Alvarez WE, Harwell JH, Resasco DE (2000) Chem Phys Lett 317:497
36. Alvarez WE, Kitiyanan B, Borona A, Resasco DE (2001) Carbon 39:547